Plasmon spectroscopy for the determination of Ti3C2Tx MXene few layer stacks architecture

T Bilyk, H-W Hsiao, R Yuan, M Benchakar, A Habrioux, Stephane Celerier, J-M Zuo, J Pacaud, V Mauchamp

Plasmon spectroscopy for the determination of $Ti_3C_2T_x$ MXene few layer stacks architecture.

T Bilyk[1], H-W Hsiao[2], R Yuan[2], M Benchakar[3], A Habrioux[3], S Célérier[3], J-M Zuo[2], J Pacaud[1] and V Mauchamp[1]

[1] Institut Pprime - UPR 3346 - CNRS, Université de Poitiers, ISAE-ENSMA, BP 30179, 86962 Futuroscope-Chasseneuil Cedex, France

[2] Department of Materials Science and Engineering, University of Illinois at Urbana-Champaign, Urbana, Illinois 61801, USA

[3] Institut de Chimie des Milieux et Matériaux de Poitiers (IC2MP), CNRS, Poitiers University , F-86073 Poitiers, France

E-mail: thomas.bilyk@univ-poitiers.fr, vincent.mauchamp@univ-poitiers.fr

Abstract. Like many 2D materials, numerous properties of MXene multilayers, and especially the most popular one $Ti_3C_2T_x$, have been shown to significantly depend on their architecture, *i.e.* the number of layers and interlayer distance. These structural parameters are thus key elements to be characterized for the analysis of MXene properties. Focusing on valence electron energy-loss spectroscopy (VEELS) as performed in a transmission electron microscope, and using density functional theory (DFT) simulations, we here analyze the layer dependent large changes in the VEEL spectra of $Ti_3C_2T_x$ multilayers as a probe of their total thickness, and emphasize the bulk plasmon energy sensitivity to interlayer distance. Together these findings allow to directly quantify the absolute number of layers in a $Ti_3C_2T_x$ stack up to $\sim$ 10 nm thickness and give access to interlayer distance modifications with sub-angström sensitivity, evidencing VEELS as a powerful method for the characterization of MXene multilayers on the nanometer scale. We expect these results to be relevant for the study of structure/properties correlations in this class of materials, especially with the development of *in situ* or environmental TEM experiments.

keywords: MXene, $Ti_3C_2T_x$, valence electron energy loss spectroscopy, TEM, Density Functional Theory simulations

Submitted to: *2D Mater.*

1. Introduction

The properties of two-dimensional (2D) materials generally depend on their architecture, *e.g.* the number of layers in a stack, the interlayer distance or the layer functionalization, as demonstrated for the band structure of graphene [1] and transition metal disulfides [2], or for the optical properties of MoS_2 [3]. MXenes [4, 5], a large family of 2D transition metal carbides and nitrides with an original combination of tunable hydrophilicity and good electrical conductivity [6], also exhibit architecture dependent properties. Because of their intrinsic properties, these materials are studied for a wide range of applications like, *e.g.* energy storage [7], transparent electrodes [8], sensors [9], or electromagnetic interference shielding [10] among many others. Focusing only on the most studied MXene compound to date, *i.e.* $Ti_3C_2T_x$ [11] (where T-groups usually correspond to O, OH, F and/or Cl surface terminations inherited from the chemical exfoliation of the MAX phases precursors [12]), it has been shown that the electrical resistivity [13], the mechanical [14] and optical [15] properties, or the electromagnetic shielding [10] have a significant dependence on the number of layers in few layer stacks. Beyond the layer number, MXene properties are also very sensitive to the interlayer distance which can be significantly increased by intercalation of ions and/or molecules [16], or reduced by annealing with the aim of removing the interlayer intercalated water [17]. Such mechanisms have been shown to have a strong impact on the electrical, optical or charge storage properties of $Ti_3C_2T_x$ for instance [15, 16, 17, 18].

The mechanisms at play in the thickness or interlayer distance dependence of the physical properties operate at a very small scale, typically on the order of the nanometer for $Ti_3C_2T_x$ (*i.e.* the thickness of a single layer [19]). In order to study these mechanisms or correlate the properties of a MXene few-layer stack to its actual architecture, one needs appropriate characterization tools, and transmission electron microscopy (TEM) is one of the very powerful ones [19, 20, 21, 22]. In addition, TEM is nowadays increasingly used to directly probe materials properties or reactivity with *in situ* or environmental experiments. Using these approaches, the dependence of Ti or (Mo,Ti)-based MXenes conductivity on interlayer species deintercalation and surface defunctionalization has been evidenced [23], the plasmonic properties of MXene flakes as a function of their shape or thickness have been probed [24, 25], the reactivity of $Ti_3C_2T_x$ flakes towards different gases has been studied [26, 27], and strong thickness dependent mechanical properties in the 20-60 nm range have been evidenced [28].

In order to take full advantage of these characterizations and clearly evidence the thickness/properties interplay in this rich family of 2D materials, one thus needs to precisely determine the architecture of a given MXene few-layer stack during TEM experiments. In this context, we show that valence EELS (VEELS) which corresponds to the excitation of the materials valence electrons, combined to density functional theory (DFT) simulations, provides a direct way to quantify the absolute number of layers in $Ti_3C_2T_x$ few layer stacks for thicknesses up to $\sim$ 10 layers, *i.e.* where the thickness/properties dependency is the most important. Unlike other 2D materials like

graphene, h-BN or transition metal dichalcogenides, where the energy position of the main plasmon peak in VEEL spectra is dependent on the number of layers [29, 30, 31], we show that it is the intensity ratio between the surface and bulk modes that provides the information on thickness in $Ti_3C_2T_x$ multilayers. In addition, although the bulk plasmon energy is insensitive to the number of layers in a $Ti_3C_2T_x$ stack, we show that it is very sensitive to the interlayer distance and can be used to monitor variations in the average interlayer distance between the MXene layers with sub-angström sensitivity, thus providing a complete description of the architecture of a few-layer stack on the nanometer scale.

2. Experimental and theoretical details

2.1. Sample preparation

The $Ti_3C_2T_x$ samples were prepared by etching aluminium from Ti_3AlC_2 MAX phase powders using a LiF+HCl etchant in soft conditions as described by Benchakar *et al* [32]. After synthesis, the MXenes were dried and stored under a N_2 atmosphere. The dried MXene clay was dispersed in water to prepare TEM samples. Hand stirring was sufficient to produce a colloidal suspension. A drop of the suspension was collected and deposited on a copper grid covered with lacy carbon films. Therefore, the studied MXene stacks are probed with the beam along the *c*-cell parameter of the multilayer, *i.e.* along the [0001] zone axis.

2.2. (S)TEM experiments

The STEM-HAADF micrographs, VEEL spectra and position averaged convergent beam electron diffraction (PACBED) patterns were acquired in a FEI Themis Z microscope, equipped with a monochromator and a GIF spectrometer. For all acquisitions, the acceleration voltage was set to 80 keV in order to minimize the potential beam damage. The spectra were acquired in TEM mode, with an energy resolution of about 0.15 eV as determined from the full width at half maximum of the zero loss peak. The collection semi-angle was measured to be around 6 mrad. For the acquisition of PACBED patterns, a CMOS camera was used, in order to decrease acquisition time and again reduce the electron beam damage. A convergence semi-angle of 2.81 mrad was used for the acquisitions. The samples, initially close to [0001] zone axis, were tilted in order to get the most symmetrical patterns. Simulations were performed using the JEMS software in precession mode [33].

2.3. DFT simulations

The energy-dependent dielectric functions of Ti_3C_2 and $Ti_3C_2T_2$ with T=O, F and OH were obtained from density functional theory (DFT) calculations. The WIEN2k code, based on the full-potential (linearized) augmented planewave plus local orbitals

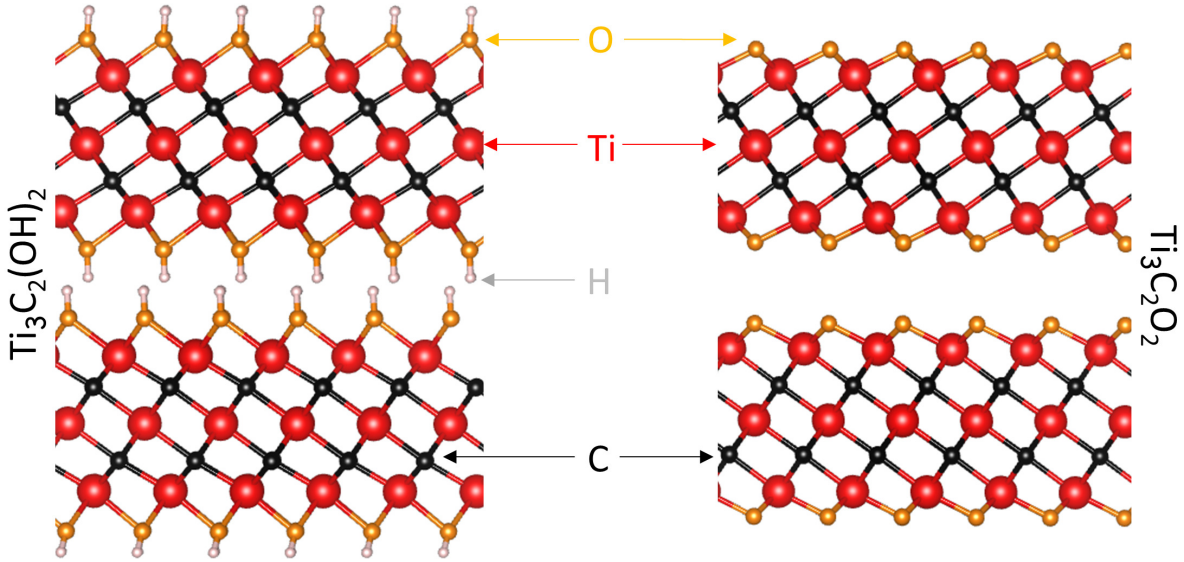

Figure 1. Side views of two superimposed MXene layers as described with the P_1 unit cell of the $Ti_3C_2(OH)_2$ system (left) and a standard $P6_3/mmc$ unit cell corresponding to $Ti_3C_2O_2$ in the present case (right). The functionalization groups sit on the most stable position on the Ti_3C_2 layers (*i.e.* the fcc position). The structural model were drawn using the VESTA software [39].

method, was used [34, 35, 36]. The generalized gradient approximation was used for the calculations, with the GGA-PBE exchange and correlation functional [37]. The basis set was converged using a $R_{MT} \times K_{max}$ product of 8 (except for $Ti_3C_2(OH)_2$ where the $R_{MT} \times K_{max}$ value was 3 due to shortest O-H bonds), R_{MT} being the smallest atomic sphere radius and K_{max} the plane-wave cut-off. For all presented results the Muffin-Tin radii are determined using the WIEN2k routine, with almost touching spheres. As the generalized gradient approximation was used, the magnitude of the largest vector in the charge-density Fourier expansion, Gmax, was set to 14. For atomic position relaxations, a grid of 10×10×2 k-points was used. After the relaxations, the self-consistent field calculations were done with an amount of 1500 k-points in the first Brillouin zone. For dielectric function calculations, 50000 k-points were used to converge the Drude frequency. A broadening of 2 eV was used for the comparison with experimental results.

For the $Ti_3C_2(OH)_2$ system, a slightly distorted unit cell as compared to the usual $P6_3/mmc$ space group was used in agreement with previous XRD Rietveld refinements [38]. It allows to minimize the overlap between the OH groups on two facing layers (see figure 1). A P1 structure was considered with the following unit cell parameters: a=b=3.058 Å, c=19.6 Å, α=93.234 ^{o}, β=87.459 ^{o} and γ=120.161 ^{o}. For the $Ti_3C_2O_2$ and $Ti_3C_2F_2$ systems, structures described in the $P6_3/mmc$ space group with the same a, b and c cell parameters gave similar electronic structure when compared to the distorted, *i.e.* triclinic, unit cell. As a consequence, the loss functions for a hexagonal and triclinic unit cell are similar for $Ti_3C_2F_2$ (see SI, figure S1). We therefore

used more simple hexagonal unit cells for the simulations of the Ti_3C_2, $Ti_3C_2O_2$ and $Ti_3C_2F_2$ systems. In addition, we also checked for $Ti_3C_2(OH)_2$ that considering a shifted hexagonal system (*i.e.* where the two layers in a hexagonal unit cell are shifted - see the structural models in SI, figure S1) did not significantly modify the obtained VEEL spectra as compared to the triclinic model. Overall, these results show a weak impact of the stacking on the VEEL spectra. As an example, the Wyckoff positions in the initial $Ti_3C_2F_2$ structure were: Ti_v in 2a position (0,0,0); Ti_s in 4f position (2/3,1/3,z_{Tis}), with z_{Tis}=0.119727; C in 4f position (2/3, 1/3,z_C), with z_C=0.565283; F in 4e (0,0,z_F), with z_F=0.183167. These structures, inherited from the MAX phase precursor, correspond to a stack of two MXene layers.

In order to increase the interlayer distances, the *c*-cell parameter was increased in the hexagonal systems. For each *c*-cell parameter, all atomic positions were relaxed, keeping the unit cell parameters fixed. These relaxations only very weakly modified the atomic positions (below 2% for the Ti-T or Ti-C distances in the most sensitive case, *i.e.* $Ti_3C_2O_2$, when changing the *c* parameter from 19.6 to 25 Å). As a consequence, the sheet thickness can be considered as almost constant in the range of interlayer distances presented here. The charge, energy and force convergences were respectively set to 0.0001 e, 0.0001 Ry and 1 mRy/a.u.

2.4. Kröger formalism and simulation of VEEL spectra

The OPTIC program of WIEN2k was used to compute the energy-dependent dielectric function for the different systems, $\varepsilon(\omega)$, in the random phase approximation [40]. Following previous studies [25, 38], and given that the MXenes were observed in the [0001] zone axis, the VEEL signal is mainly determined by the basal component of the dielectric tensor. The VEEL spectra were thus calculated using only this component of $\varepsilon(\omega)$. From this quantity, the low losses are usually determined from the loss function $Im\left(\frac{-1}{\varepsilon(\omega)}\right)$. However in order to compute the thickness dependent low losses, the differential energy loss as derived from the Kröger theory was used [41, 42]. Experimental parameters such as the acceleration voltage of 80 keV or the collection semi-angle of 6 mrad were needed. The convergence semi-angle was set to 0 as we used parallel illumination in TEM mode.

3. Results and discussion

Figure 2-a) presents normalized valence EEL spectra acquired on five $Ti_3C_2T_x$ multilayer flakes with different thicknesses. The spectra were acquired in TEM mode on large areas, *i.e.* typically several hundreds of nanometers in diameter. They were normalized on the 24 to 29 eV energy range so that the integrated intensity equals to 10000. The STEM-HAADF micrographs corresponding to samples 1 to 5 are given in figures 2-b) to f) respectively with the green circles evidencing the areas probed in EELS. These micrographs evidence large flakes with sharp edges and uniform contrast, which can

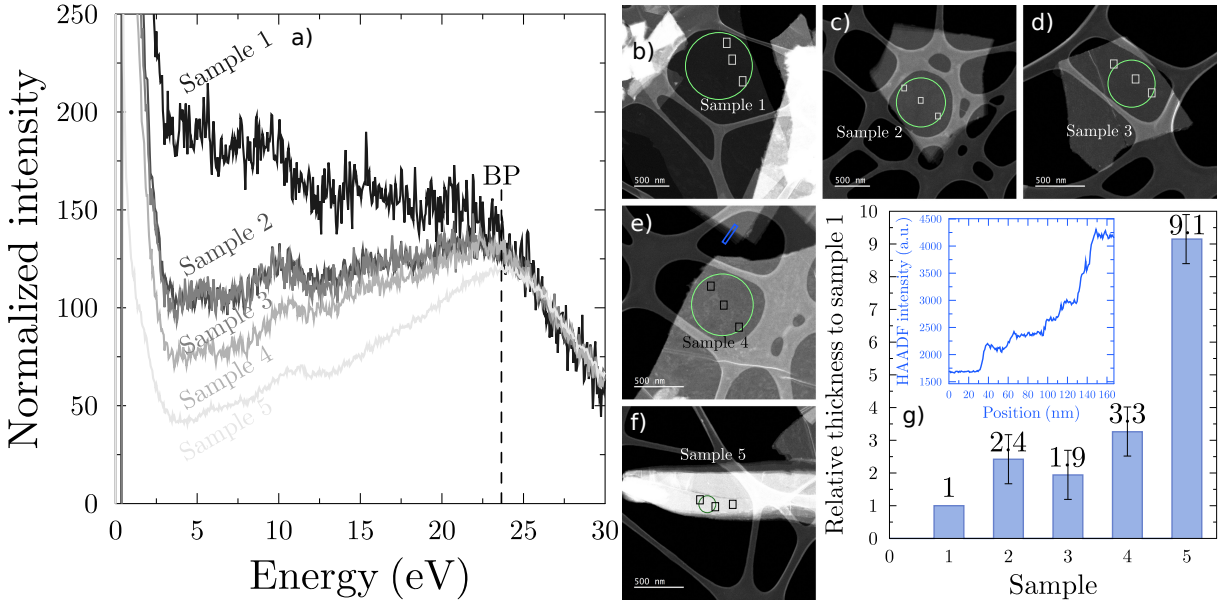

Figure 2. a) Experimental VEEL spectra recorded on $Ti_3C_2T_x$ MXene stacks with different thicknesses, *i.e.* with different number of layers. Spectra were normalized so as to have an integrated intensity equal to 10000 on the 24 to 29 eV energy range. b) to f) STEM-HAADF micrographs of the corresponding investigated areas: green circles represent the zones where the VEEL spectra were acquired, squares where PACBED patterns were recorded (see supporting information). g) Average intensities measured in the STEM-HAADF micrographs. Intensity ratios taking the sample 1 as a reference are given. Error bars correspond to the intensity mean square error measured over the probed areas. Inset: intensity steps recorded along the blue rectangle in e).

be easily obtained by the MILD method developed by Alhabeb *et al.* [43] and used in this work. It is well known that STEM-HAADF intensities measured in a sample is proportional to its thickness, *i.e.* the quantity of matter crossed by the electrons. This fact was checked for graphene in stacks with up to 50 sheets [44]. Therefore, the intensities measured in figures 2-b) to f) clearly show that the flakes have different thicknesses. The relative thicknesses between the different samples are given in figure 2-g), taking the thinnest sample as a reference, *i.e.* the sample 1 in the present case. Knowing the exact number of MXene flakes in sample 1, one would be able to approximately determine the number of layers in samples 2 to 5 from these HAADF intensities. As evidenced in figure 2-g) the error bars in STEM-HAADF intensities are however significant, pointing out a non-negligible error in the determination of the stack thickness using this data set: differentiate samples 2, 3 and 4 is difficult. The inset shows the typical steps observed on the edge of a stack (see the blue rectangle in figure 2-e), with an observed minimal intensity step of about 300 counts.

From VEEL spectra, the sample thickness (t) is often estimated using the *Log-Ratio* technique, which provides a thickness relative to the inelastic scattering mean free path (λ) of the incident electron in the sample [45]. The t/λ values, extracted from the spectra given in figure 2-a recorded over a 100 eV energy range, are 0.08,

0.1, 0.1, 0.15 and 0.28 for the samples 1 to 5 respectively. This method requires the knowledge of λ to obtain absolute thicknesses. This parameter is not accurately known for our experimental conditions and it should be estimated using different models. Two analytical expressions are widely used: a first one determined by Malis *et al.* [46] where the specimen is characterized by an effective atomic number ($Z_{eff} = \frac{\sum_i f_i Z_i^{1.3}}{\sum_i f_i Z_i^{0.3}}$ with Z_i the atomic number of each element with atomic fraction f_i) and a second one determined by Iakoubovskii et al. [47] where the specimen is characterized by its density. These two expressions do not give the same value for λ for a given material and, considering a Ti_3C_2OF composition, one obtains $\lambda_{Malis} = 88$ nm and $\lambda_{Iakoubovskii} = 100$ nm for our experimental conditions (*i.e.*, 80 kV voltage, parallel illumination and 6 mRad collection semi-angle). Other surface compositions, like $Ti_3C_2F_2$, $Ti_3C_2O_2$ and $Ti_3C_2(OH)_2$ give very similar λ values as described in SI. The estimated uncertainty is typically between 10 and 20 % for these models [48]. As discussed in the SI, the absolute thicknesses obtained using this approach are only approximate for samples 2 to 4 and is largely overestimated for sample 1, by more than a factor of 2: the log-ratio method gives a 7 to 8 layers thick sample whereas the true thickness is 3 layers as evidenced latter. Given the uncertainty on λ and the fact that the *Log-Ratio* technique was shown to be unreliable for very low thicknesses [45, 49], *i.e.* when the contribution of surface excitations become significant, these discrepancies are not surprising and underline the need for a more accurate approach for the characterization of the number of layers in the thinnest areas.

Coming back to figure 2-a), a clear tendency appears on the evolution of the VEEL spectra of MXene stacks for increasing thicknesses: the thinner the MXene stack, the lower the intensities of the bulk plasmon (labelled BP in figure 2-a)) as compared with the intensities recorded at lower energy, *i.e.* typically below 15 eV. In addition, in sharp contrast with other 2D materials, the BP energy does not significantly change with the thickness. These data, fully consistent with previously published results [25], confirm the findings that the low loss region in $Ti_3C_2T_x$ can be analyzed in terms of two contributions: the bulk one, corresponding to the loss function $\mathrm{Im}\left(\frac{-1}{\varepsilon}\right)$ with $\varepsilon(\omega)$ the energy dependent dielectric permittivity of the sample and which gives the main peak around 23.5 eV; and the surface modes at lower energy that can be described using different formalisms like, *e.g.* the original approach of R. F. Ritchie or the description of E. Kröger which includes retardation effects [50, 41]. When the thickness increases, the bulk plasmon is more sharply visible as shown in figure 2.a).

To obtain the absolute thickness from the experimental VEEL spectra of samples 1 to 5, we compared these data with simulated ones obtained using DFT calculations of $\varepsilon(\omega)$ as input to the Kröger cross section as described in the theoretical details. Specific attention was paid to find the structural parameters giving simulated spectra the closest to experimental ones. The effect of surface terminations, which play an important role on the properties of 2D materials and particularly in MXenes [32, 51, 52, 53, 54, 55, 56, 57], was first investigated. The simulated low loss spectra presented in figure 3.a) were

calculated for a multilayer thickness of 30 nm for which the main contribution comes from the loss function. These spectra are compared to the VEEL spectrum collected on the thicker zone, *i.e.* the sample 5. They confirm the high sensitivity of the MXene electronic structure to their surface functionalization. In particular, it can be noticed that the bulk plasmon energy decreases significantly from $Ti_3C_2(OH)_2$ to $Ti_3C_2O_2$, $Ti_3C_2F_2$ and Ti_3C_2. Secondly, it is shown that the best agreement is obtained when considering layers terminated with hydroxyl groups in the simulation, with an almost perfect match with the experiment in the 10 to 30 eV energy range. Although (OH) groups are not expected to be the most numerous ones for $Ti_3C_2T_x$ [32], this system will be used in the future developments. It is not clear at the moment why the $Ti_3C_2(OH)_2$ model gives the best agreement with the experiment, but this was already observed for HF prepared samples [25, 38]. A possible reason could be related to the fact that a true MXene structure is much more complicated than the simplified structures presented in figure 1. In particular, it is well known that water molecules are confined in between the MXene layers and have an important impact on the architecture of MXene stacks and physical/chemical properties of MXenes [17]. From these considerations, one can assume that considering OH terminated MXene improves the agreement with experimental spectra by allowing to, somehow, consider the interlayer hydrogen or OH bonds coming from confined water molecules and their interaction with the MXene surface.

Figure 3.b) shows the evolution of the simulated low loss spectra as a function of the MXene stack thickness, *i.e.* when changing the sample thickness in the Kröger formula. For these simulations, the thickness of a single $Ti_3C_2T_x$ layer was considered to be 1 nm, following high resolution TEM measurements [19]. The thickness sensitivity is particularly important from 1 to 10 nm, *i.e.* 1 to 10 layers, mostly due to the evolution of the surface contribution as shown by the dashed curves in the figure. Like other properties in 2D materials, when the thickness increases the VEEL spectrum converges towards the bulk one. For comparison, the experimental spectra of figure 2-a are also reported in figure 3-b: a superimposition good enough to obtain thickness measurements by eye on samples 1, about 3 layers, and samples 2 and 3, about 7 or 8 layers, is evidenced.

To be more quantitative, the mean squared error (MSE) between the experimental spectra and the simulated ones considering thicknesses in the 1 to 30 layers range, was calculated. These MSE are represented as a function of the number of layers in the simulated stacks in the figure 3.c). The curves clearly present a minimum except for sample 5. The deduced thickness measurements for the samples 1, 2, 3 and 4 are respectively 3, 7, 7 and 12 layers. The quality of the overlap between simulated and experimental curves confirm the accuracy of the thickness measurement. In order to estimate the uncertainty of these measurements, the same approach was used considering four different intervals for the MSE: from 5 to 10 eV; 10 to 15 eV; 15 to 20 eV; and 20 to 25 eV. When focusing on the first three intervals, the most thickness sensitive, the uncertainty is below 0.5 nm for the sample 1, 2 and 3 and below 1 nm for the sample 4. It can be noticed from figure 3.b) that a slight underestimation of the pre-bulk plasmon

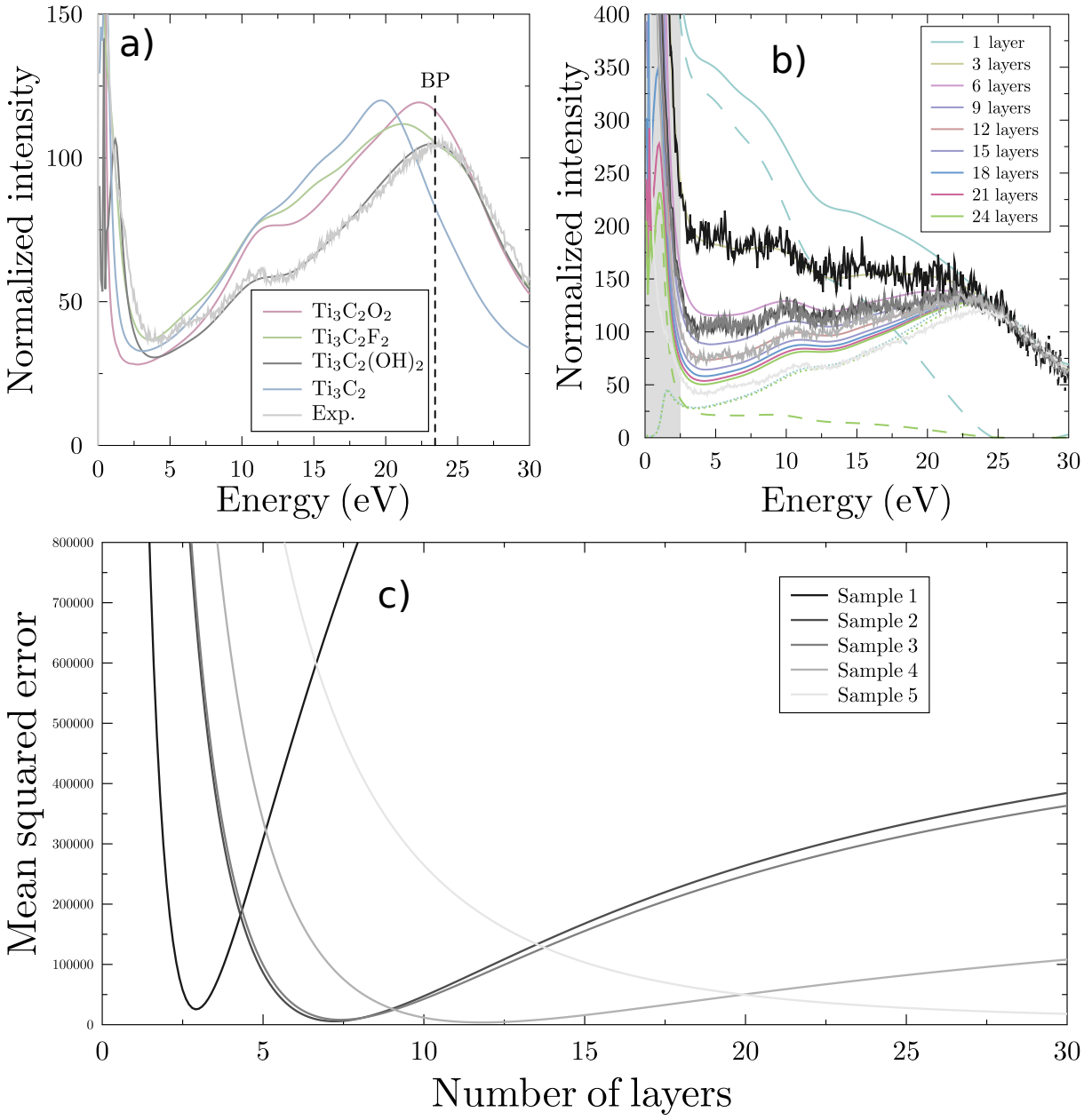

Figure 3. a-b) Simulations of $Ti_3C_2T_x$ VEEL spectra when varying a) the termination populations for a 30 layers thick stack and b) the number of layers in $Ti_3C_2(OH)_2$ stacks. Dashed and dotted lines correspond respectively to the surface and volume contributions to the EEL spectra for both 1 (pastel blue) and 24 (green) layers thick $Ti_3C_2T_x$ MXene stacks. Experimental spectra of figure 2-a), zero loss subtracted, are also reported for qualitative comparison. For comparison, theoretical and experimental spectra were normalized in the 24-29 eV energy range so as to have an integrated intensity of 10000 in this energy range. Grey areas are disregarded because subject to difficult zero loss peak extraction. c) Mean squared error between the experimental spectra and the simulated ones for different thicknesses.

intensity is observed, leading to a slightly larger error in the last interval. However, the dotted and dashed curves show that the thickness dependence is weak in that interval.

The width of the minima in figure 3-c) increase with the thickness of the investigated stack. This is due to the higher sensitivity of the bulk versus surface contributions ratio in low loss spectra at low thicknesses. It makes this approach more discriminant at low thicknesses contrary to the Log-Ratio method for the determination of the t/λ. The larger width of the sample 4 MSE curve is consistent with the previous discussion on uncertainty: the error on the measurement becomes close to 1 layer for that thicker sample. The number of layers in the fifth sample could not be determined since the difference between simulated spectra for high thicknesses are too low to find a minimum in the MSE curve. When the thickness increases, the measurement becomes more challenging. Fortunately, an accurate measurement of the stack thickness is much more relevant at low thicknesses where the dependence of the properties on the number of MXene layers is exacerbated.

Taking the thickness of sample 1, measured as three layers, the HAADF intensity ratios of figure 2-f) give 7.5±2, 6±2, 10±2 and 27.5±3 layers for samples 2 to 5 respectively. Although less accurate due to the error bars on the HAADF intensities, these values are in good agreement with those extracted from the VEEL spectra for samples 2 to 4, confirming the validity of our VEELS approach (see SI figure S2). At very low thickness, *i.e.* typically below 10 layers, our method is expected to unambiguously give the exact number of layers in a stack, which underlines its huge appeal. Above this value, the uncertainty is estimated to exceed 1 layer and increases with thickness. Moreover, the fact that sample 1 corresponds to a stack of three layers shows that the step of 300 counts discussed in the inset of figure 2.g) corresponds to an increase of one MXene layer in our experimental conditions. These results have also been confirmed using PACBED, CBED being a reference method for the determination of sample thickness in TEM [58, 59]. PACBED data acquisition and processing are described in supplementary information and the main conclusion is that the thicknesses of the samples 2 and 3 are confirmed to be between 5 and 8 nm, the PACBED patterns of samples 4 and 5 being unexploitable.

The thickness measurement method presented above requires DFT simulations of the dielectric function as an input to the Kröger cross section. However, inspection of the experimental and theoretical spectra given in figure 3 shows that they exhibit a roughly linear behavior in the 5-24 eV energy range. The slope dependence of linear fits of the VEEL simulated spectra as a function of the thickness was thus investigated in order to provide a simpler way to measure the thickness of a given stack from VEEL spectra. The corresponding results are presented in Figure 4. It should be noted that the slope depends on the normalization, which was here performed between 24 and 29 eV. Different collection semi-angles and acceleration voltages corresponding to standard TEM-EELS acquisition conditions were also considered in order to provide reference curves for other experimental conditions (additional curves corresponding to acceleration voltages of 200 kV and 300kV are given in supplementary information).

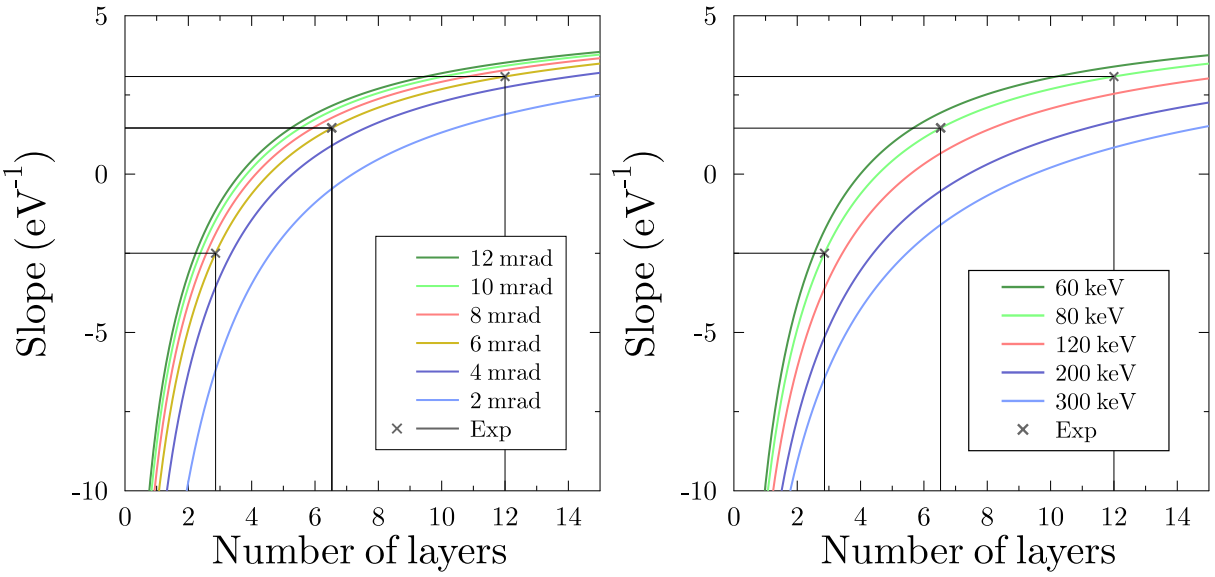

Figure 4. Slope of linear fits performed on the 5 to 24 eV energy interval on the simulated spectra (full lines) as a function of the number of layers in a stack. Slopes obtained from the fits of the experimental ones are reported as grey crosses. Lines are a guide for the eyes. Comparison of the slope thickness dependence to (left) different collection semi-angles at 80 keV and (right) to different acceleration voltages for a collection semi-angle of 6 mrad.

Results of equivalent fits performed on the experimental spectra of samples 1 to 4 are also reported as grey crosses in the figures for our experimental conditions. The values deduced from these curves are fully consistent with those obtained from the MSE with the sample 1 measured to be 3 layers thick, samples 2 and 3 close to 7 nm (within the 0.5 layer uncertainty) and sample 4 measured to be 12 layers thick. These results show that the number of layers in a stack can directly be deduced from the slope of the linear fits of the experimental spectra in the 5 to 24 eV interval.

Although confirming the possibility to generalize this approach to other MXenes would require equivalent in-depth analysis as that proposed in the present paper, we would like to stress here that we observe a behavior similar to that reported for $Ti_3C_2T_x$ (*i.e.* thickness insensitive bulk plasmon energy and surface to bulk mode ratio changing as a function of thickness) in V_2CT_x and Ti_2CT_x (see SI, figure S7, for the case of Ti_2CT_x). As a consequence, one can infer that the physics behind the VEEL spectra in these MXenes is similar to that discussed for $Ti_3C_2T_x$ so that our approach is probably generalizable to other MXenes.

As discussed previously, the interlayer spacing is also a key structural parameter with a major effect on the MXene properties. We thus investigated the possibility to probe this parameter using VEELS. The figures 5.a-c) present the evolution of the bulk plasmon energy simulated for $Ti_3C_2T_2$ MXenes when the *c*-cell parameter is increased in the hexagonal unit cells (*i.e.*, for the layers covered with fluorine, oxygen or no termination). Increasing the *c*-cell parameter results in the augmentation of the distance

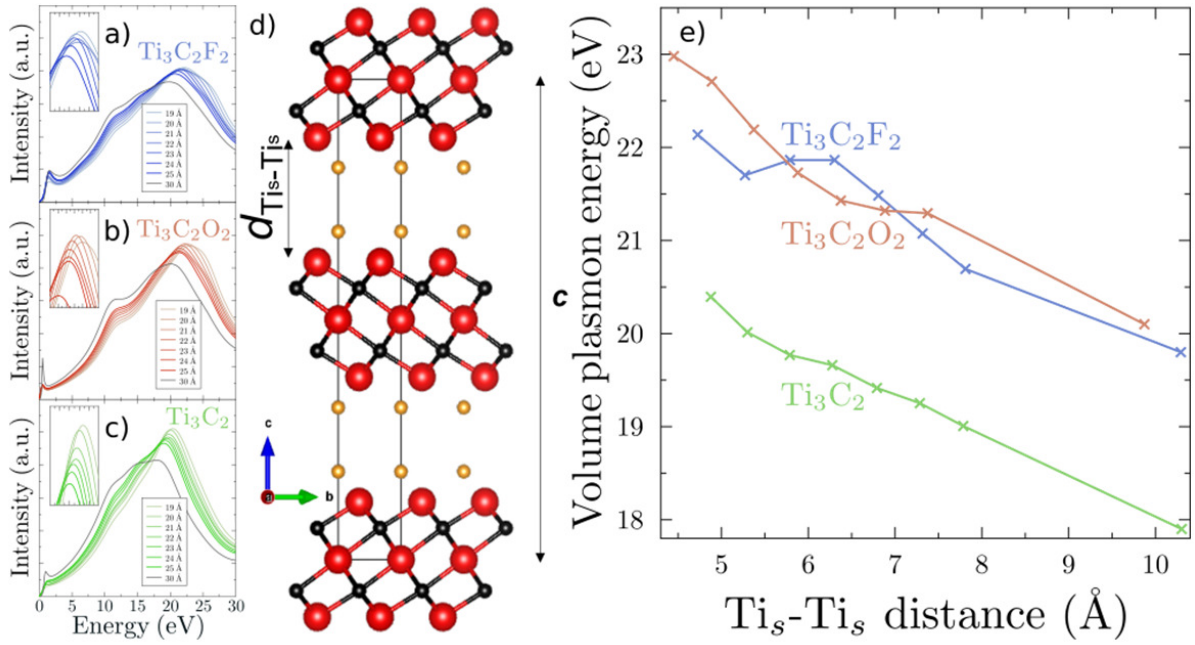

Figure 5. Evolution of simulated low loss spectra of a) $Ti_3C_2F_2$, b) $Ti_3C_2O_2$ and c) Ti_3C_2 30 layers thick MXene stacks, when changing the *c*-cell parameter and hence the interlayer distance. For each *c*-cell parameter given in the legends of figures a)-c), all atomic positions were relaxed, keeping the unit cell parameters fixed, and leading to the relaxed Ti_s-Ti_s distances presented in e). d) Sketch of the MXene unit cell as observed along the $\langle\ 100\ \rangle$ direction, and evidencing the $d_{Tis-Tis}$ distance used as a marker of the interlayer distance. e) Evolution of the bulk plasmon energy as a function of $d_{Tis-Tis}$.

between the two $Ti_3C_2T_2$ layers forming the unit cell. This distance is here characterized by $d_{Tis-Tis}$, the distance between the surface titanium atoms facing each other in the two superimposed layers as shown in figure 5.d).

One can see that the BP energy decreases when the interlayer distance increases and that the BP intensity tends to decrease. The evolution of the bulk plasmon energy as a function of the $d_{Tis-Tis}$ is presented in figure 5.e) for the $Ti_3C_2F_2$, $Ti_3C_2O_2$ and Ti_3C_2 systems. Regardless of the surface population, a decrease of around 2.5 eV is observed when increasing the interlayer distance by $\sim$ 5 Å, corresponding to *c*-cell parameters ranging from 19 to 30 Å. The slopes of the linear fits of these curves are -0.43 eV/Å, -0.52 eV/Å and -0.44 eV/Å for the $Ti_3C_2F_2$, $Ti_3C_2O_2$ and Ti_3C_2 systems respectively. These results were confirmed for the more complex and computer time demanding $Ti_3C_2(OH)_2$ system since calculations performed for $c = 20$ and 25 Å lead to a 0.53eV/Å slope. The interlayer distance sensitivity of the bulk plasmon energy in a stack can thus be used to evaluate the average distance between different layers, or characterize relative changes of it, on a very local scale. Assuming a 0.25 eV accuracy on the determination of the bulk plasmon energy and an average slope of -0.5 eV/Å for the plasmon energy evolution as a function of $d_{Tis-Tis}$, this approach offers the

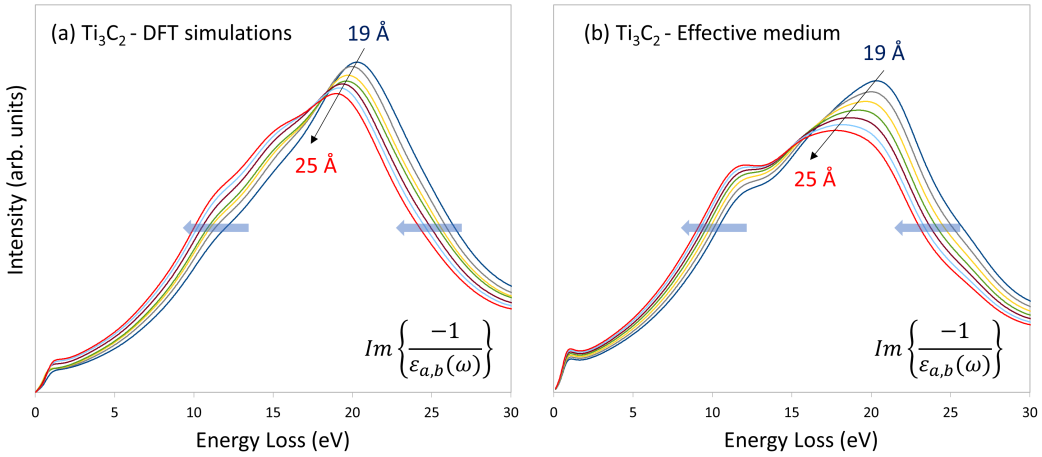

Figure 6. (a) DFT simulations of the loss function of Ti_3C_2 with a c cell unit cell parameter varying from 19 to 25 Å. (b) Corresponding results obtained in the effective medium approach, *i.e.* considering an increasing percentage of vacuum between the TiC layers.

possibility to measure 0.5 Å interlayer variations in a $Ti_3C_2T_x$ stack. Having access to this structural parameter, especially with such a resolution, is rather challenging in TEM experiments since MXene multilayers extracted from MXene powder samples generally settle parallel to the TEM grid (*i.e.* along the {0001} zone axis) so that imaging or diffraction techniques essentially probe the in-plane structure. Using the bulk plasmon energy shift to directly detect local variations in the interlayer distances is thus very interesting given the crucial role played by this structural parameter on MXene stacks properties [16, 18, 17] .

Focusing on Ti_3C_2, the dependence of the bulk plasmon energy on the c parameter can be understood using an effective medium (EM) approach, where the MXene stack is described as an alternance of TiC layers and vacuum. The respective thicknesses of the TiC layers and vacuum ones are d and $c/2$-d, with c the unit cell parameter of the Ti_3C_2 hexagonal structure. In this approach, the two components of the hexagonal dielectric tensor, *i.e.* $\varepsilon_{a,b}(\omega)$ for the basal plane and $\varepsilon_c(\omega)$ along the c axis, are then given by [60]:

$$\varepsilon_{a,b}(\omega) = \frac{d}{c/2}\varepsilon_{TiC}(\omega) + \frac{c/2-d}{c/2}\varepsilon_{vac}(\omega) \quad (1)$$

$$\frac{1}{\varepsilon_c(\omega)} = \frac{d}{c/2}\frac{1}{\varepsilon_{TiC}(\omega)} + \frac{c/2-d}{c/2}\frac{1}{\varepsilon_{vac}}(\omega) \quad (2)$$

with ε_{vac} and ε_{TiC} the dielectric permittivities of vacuum and TiC respectively. Figure 6 shows that the EM approach qualitatively reproduces the evolution of the VEEL spectra obtained from DFT when varying the c-cell parameter with a global red shift of the low loss spectrum resulting in a red shift of the BP energy. One can however notice that this shift is slightly overestimated by the EM approach and that it does

not reproduce the double peak between 10 and 15 eV (only the peak around 11.5 eV is reproduced). Given the simplicity of the EM model, it is not surprising that it does not capture all the details of the electronic structure of the Ti_3C_2 MXene stack. Besides these discrepancies, the EM results show that the bulk plasmon energy reduction can be simply understood in terms of an increase of the quantity of vacuum in the stack which results in a decrease of the number of valence electrons per unit volume in the system. This last parameter is key to the determination of the plasma frequency according to the Drude model.

4. Conclusion

In summary, we have shown that, using the significant thickness dependence of the EELS cross section in the low loss part of the spectrum, it is possible to exactly quantify the number of layers in $Ti_3C_2T_x$ multilayers for thicknesses below ~ 10 nm. This can be done by comparison with simulations involving the energy dependent dielectric function of the material obtained from DFT, but also more simply from the thickness dependence of the slope of linear fits of the experimental spectra in a well-chosen energy range. In addition, DFT simulations show that monitoring the bulk plasmon shift in these materials also offers the possibility to probe the evolution of the average interlayer distance in a stack with sub-angström resolution, thereby providing the architecture of a $Ti_3C_2T_x$ multilayer stack on the nanometer scale in the TEM.

Compared to other techniques, we believe that using VEELS presents several interesting features. First, because it is dominated by the bulk plasmon excitation which corresponds to the excitation of the whole valence electron gas, we do not expect small molecular-like impurities to significantly modify the VEEL spectra of MXenes obtained with different etching conditions, the latter being known to have a large impact on the nature and amount of secondary phases present in the material [15,32]. This was recently confirmed on $Ti_3C_2T_x$ where the VEEL spectra obtained on flakes synthesized with different etchants were shown to be very similar [22]. In addition, our approach has two other important features compared to other TEM-based methods. First, it allows in a single measurement in plane-view, which is the natural way that MXene sheets are supported on the TEM grid, to have both an information on the number of layers and the interlayer spacing. This is hardly possible with electron imaging or diffraction techniques. In addition, the VEEL spectra being weakly sensitive to slight sample misorientations with respect to the electron beam, the acquisition and interpretation of exploitable data are rather straightforward.

5. Acknowledgements

The authors acknowledge financial support from the "Région Nouvelle Aquitaine" for the Ph.D thesis of T. Bilyk, the SIMME doctoral school for supporting T. Bilyk's stay at the University of Illinois, the French research ministry for the Ph.D. thesis of

M. Benchakar, and the "Agence National de la Recherche" (reference ANR-18-CE08-014 – MXENECAT project). This work was supported by the French government program "Investissements d'Avenir" (EUR INTREE, reference ANR-18-EURE-0010). JMZ is partially supported by DOE DE-SC0022060 and RLY was supported by Intel Corporation through an SRC project (Award 54071821). Computations have been performed on the supercomputer facilities of the Mesocentre de calcul de Poitou Charentes. Pr. P. Moreau (IMN, Nantes) is gratefully acknowledged for making available his code allowing the computation of the Kröger cross section.

6. References

[1] Ohta T, Bostwick A, McChesney J L, Seyller T, Horn K and Rotenberg E 2007 Interlayer Interaction and Electronic Screening in Multilayer Graphene Investigated with Angle-Resolved Photoemission Spectroscopy *Phys. Rev. Lett.* **98** 206802

[2] Kuc A, Zibouche N and Heine T 2011 Influence of quantum confinement on the electronic structure of the transition metal sulfide TS_2 *Phys. Rev. B* **83** 245213

[3] Mak K F, Lee C, Hone J, Shan J and Heinz T F 2010 Atomically Thin MoS_2: A New Direct-Gap Semiconductor *Phys. Rev. Lett.* **105** 136805

[4] Anasori B and Gogotsi, Y 2017 2D Metal Carbides and Nitrides (MXenes) Structure, Properties and Applications *Springer*

[5] VahidMohammadi A, Rosen J and Gogotsi Y 2021 The world of two-dimensional carbides and nitrides (MXenes) *Science* **372** eabf1581

[6] Ghidiu M, Lukatskaya M R, Zhao M Q, Gogotsi Y and Barsoum M W 2014 Conductive two-dimensional titanium carbide 'clay' with high volumetric capacitance *Nature* **516** 78-81

[7] Anasori B, Lukatskaya M R and Gogotsi Y 2017 2D metal carbides and nitrides (MXenes) for energy storage *Nature Reviews Materials* **2** 16098

[8] Zhang C J and Nicolosi V 2019 Graphene and MXene-based transparent conductive electrodes and supercapacitors *Energy Storage Materials* **16** 102-125.

[9] Pei Y, Zhang X, Hui Z, Zhou J, Huang X, Sun G and Huang W 2021 $Ti_3C_2T_x$ MXene for Sensing Applications: Recent Progress, Design Principles, and Future Perspectives *ACS Nano* **15** 3996-4017

[10] Yun T, Kim H, Iqbal A, Cho Y S, Lee G S, Kim M K, Kim S J, Kim D, Gogotsi Y, Kim S O and Koo C M 2020 Electromagnetic Shielding of Monolayer MXene Assemblies *Adv. Mater.* **32** 1906769

[11] Gogotsi Y and Anasori B 2019 The Rise of MXenes *ACS Nano* **13** 8491-8494

[12] Barsoum M W 2013 MAX Phases: Properties of Machinable Ternary Carbides and Nitrides *Wiley*

[13] Sang X, Xie Y, Lin M W, Alhabeb M, Van Aken K L, Gogotsi Y, Kent P R C, Xiao K and Unocic R R 2016 Atomic Defects in Monolayer Titanium Carbide ($Ti_3C_2T_x$) MXene *ACS Nano* **10** 9193-9200.

[14] Lipatov A, Lu H, Alhabeb M, Anasori B, Gruverman A, Gogotsi Y and Sinitskii A 2018 Elastic properties of 2D $Ti_3C_2T_x$ MXene monolayers and bilayers *Science Advances* **4** eaat0491

[15] Halim J, Lukatskaya M R, Cook K M, Lu J, Smith C R, Näslund L Å, May S J, Hultman L, Gogotsi Y, Eklund P and Barsoum M W 2014 Transparent Conductive Two-Dimensional Titanium Carbide Epitaxial Thin Films *Chem. Mater* **26**, 2374-2381

[16] Luo J, Zhang W, Yuan H, Jin C, Zhang L, Huang H, Liang C, Xia J, Zhang J, Gan Y

and Tao X 2017 Pillared Structure Design of MXene with Ultralarge Interlayer Spacing for High-Performance Lithium-Ion Capacitors *ACS Nano* **11** 2459-2469.

[17] Célérier S, Hurand S, Garnero C, Morisset S, Benchakar M, Habrioux A, Chartier P, Mauchamp V, Findling N, Lanson B and Ferrage E 2019 Hydration of $Ti_3C_2T_x$ MXene: An Interstratification Process with Major Implications on Physical Properties *Chem. Mater* **31** 454-461.

[18] Hantanasirisakul K, Zhao M Q, Urbankowski P, Halim J, Anasori B, Kota S, Ren C E, Barsoum M W and Gogotsi Y 2016 Fabrication of $Ti_3C_2T_x$ MXene Transparent Thin Films with Tunable Optoelectronic Properties *Adv. Electron. Mater.* **2** 1600050

[19] Shekhirev M, Shuck C E, Sarycheva A and Gogotsi Y 2021 Characterization of MXenes at every step, from their precursors to single flakes and assembled films *Progress in Materials Science* **120** 100757

[20] Alnoor H, Elsukova A, Palisaitis J, Persson I, Tseng E N, Lu J, Hultman L and Persson P O Å 2021 Exploring MXenes and their MAX phase precursors by electron microscopy *Materials Today Advances* **9** 100123

[21] Persson I, Näslund L Å, Halim J, Barsoum M W, Darakchieva V, Palisaitis J, Rosen J and Persson P O A 2017 On the organization and thermal behavior of functional groups on Ti_3C_2 MXene surfaces in vacuum *2D Materials* **5** 015002

[22] Bilyk T, Benchakar M, Bugnet M, Loupias L, Chartier P, Pazniak H, David M L, Habrioux A, Celerier S, Pacaud J and Mauchamp V 2020 Electronic Structure Sensitivity to Surface Disorder and Nanometer-Scale Impurity of 2D Titanium Carbide MXene Sheets as Revealed by Electron Energy-Loss Spectroscopy *J. Phys. Chem. C* **124** 27071-27081

[23] Hart J L, Hantanasirisakul K, Lang A C, Anasori B, Pinto D, Pivak Y, van Omme J T, May S J, Gogotsi Y, Taheri M L 2020 Control of MXenes' electronic properties through termination and intercalation *Nat. Commun.* **10** 522

[24] El-Demellawi J K, Lopatin S, Yin J, Mohammed O F and Alshareef H N 2018 Tunable Multipolar Surface Plasmons in 2D $Ti_3C_2T_x$ MXene Flakes *ACS Nano* **12** 8485-8493

[25] Mauchamp V, Bugnet M, Bellido E P, Botton G A, Moreau P, Magne D, Naguib M, Cabioc'h T and Barsoum M W 2014 Enhanced and tunable surface plasmons in two-dimensional Ti_3C_2 stacks: Electronic structure versus boundary effects *Phys. Rev. B* **89** 235428

[26] Persson I, Halim J, Hansen T W, Wagner J B, Darakchieva V, Palisaitis J, Rosen J and Persson P O Å 2020 How Much Oxygen Can a MXene Surface Take Before It Breaks? *Adv. Funct. Mater.* **30** 1909005

[27] Persson I, Halim J, Lind H, Hansen T W, Wagner J B, Näslund L Å, Darakchieva V, Palisaitis J, Rosen J and Persson P O Å 2019 2D Transition Metal Carbides (MXenes) for Carbon Capture *Adv. Mater.* **31** 1805472

[28] Firestein K L, von Treifeldt J E, Kvashnin D G, Fernando J F S, Zhang C, Kvashnin A G, Podryabinki E V, Shapeev A V, Siriwardena D P, Sorokin P B and Golberg D 2020 Young's Modulus and Tensile Strength of Ti_3C_2 MXene Nanosheets As Revealed by In Situ TEM Probing, AFM Nanomechanical Mapping, and Theoretical Calculations. *Nano Lett. 20* 5900-5908

[29] Eberlein T, Bangert U, Nair R R, Jones R, Gass M, Bleloch A L, Novoselov K S, Geim A and Briddon P R 2008 Plasmon spectroscopy of free-standing graphene films *Phys. Rev. B* **77** 233406

[30] Johari P and Shenoy V B 2011 Tunable Dielectric Properties of Transition Metal Dichalcogenides *ACS Nano* **5** 5903-5908

[31] Pan C T, Nair R R, Bangert U, Ramasse Q, Jalil R, Zan R, Seabourne C R and Scott A J 2012 Nanoscale electron diffraction and plasmon spectroscopy of single- and few-layer boron nitride *Phys. Rev. B* **85** 045440

[32] Benchakar M, Loupias L, Garnero C, Bilyk T, Morais C, Canaff C, Guignard N, Morisset

S, Pazniak H, Hurand S, Chartier P, Pacaud J, Mauchamp V, Barsoum M W, Habrioux A and Célérier S 2020 One MAX phase, different MXenes: A guideline to understand the crucial role of etching conditions on $Ti_3C_2T_x$ surface chemistry *Applied Surface Science* **530** 147209

[33] Stadelmann P A Java version of electron microscopy software. Available at https://www.jems-swiss.ch/

[34] Cottenier S 2014 Density Functional Theory and the Family of (L)APW-methods: a step-by-step introduction. *http://www.wien2k.at/reg user/textbooks/DFT and LAPW 2nd.pdf*

[35] Blaha P, Schwarz K, Tran F, Laskowski R, Madsen G K H and Marks L D 2019 WIEN2k: An Augmented Plane Wave plus Local Orbitals Program for Calculating Crystal Properties. *Technische Universität Wien*

[36] Blaha P, Schwarz K, Tran F, Laskowski R, Madsen G K H and Marks L D 2020 WIEN2k: An APW+lo program for calculating the properties of solids. *J. Chem. Phys.* **152** 074101

[37] Perdew J P, Burke K and Ernzerhof M 1996 Generalized Gradient Approximation Made Simple *Phys. Rev. Lett.* **77** 3865-3868

[38] Magne D, Mauchamp V, Célérier S, Chartier P and Cabioc'h T 2015 Spectroscopic evidence in the visible-ultraviolet energy range of surface functionalization sites in the multilayer Ti_3C_2 MXene *Phys. Rev. B* **91** 201409

[39] Momma K and Izumi F 2011 *VESTA3* for three-dimensional visualization of crystal, volumetric and morphology data *J. Appl. Cryst.* **44** 1272-1276

[40] Ambrosch-Draxl C and Sofo J O 2006 Linear optical properties of solids within the full-potential linearized augmented planewave method *Computer Physics Communications* **175** 1-14.

[41] Kröger E 1970 Transition radiation, Cerenkov radiation and energy losses of relativistic charged particles traversing thin foils at oblique incidence *Zeitschrift für Physik* **235** 403-421

[42] Stöger-Pollach M 2008 Optical properties and bandgaps from low loss EELS: Pitfalls and solutions *Micron* **39** 1092-1110

[43] Alhabeb M, Maleski K, Anasori B, Lelyukh P, Clark L, Sin S and Gogotsi Y 2017 Guidelines for Synthesis and Processing of Two-Dimensional Titanium Carbide ($Ti_3C_2T_x$ MXene) *Chem. Mater.* **29** 7633-7644

[44] Song F Q, Li Z Y, Wang Z W, He L, Han M, Wang G H 2010 Free-standing graphene by scanning transmission electron microscopy *Ultramicroscopy* **110** 1460-1464

[45] Egerton R F 2011 Electron Energy-Loss Spectroscopy in the Electron Microscope *Springer*

[46] Malis T, Cheng S C and Egerton R F 1988 EELS log-ratio technique for specimen-thickness measurement in the TEM *J. Elec. Microsc. Tech.* **8** 193-200

[47] Iakoubovskii K, Mitsuishi K, Nakayama Y and Furuya K 2008 Thickness measurements with electron energy loss spectroscopy *Microsc. Res. Tech.* **71** 626-631

[48] Yesibolati M N, Laganá S, Kadkhodazadeh S, Mikkelsen E K, Sun H, Kasama T, Hansen O, Zaluzec N J and Mølhave K 2020 Electron inelastic mean free path in water *Nanoscale* **12** 20649-20657

[49] Batson P E 1993 Silicon $L_{2,3}$ near-edge fine structure in confined volume *Ultramicroscopy* **50** 1-12

[50] Ritchie R H 1957 Plasma Losses by Fast Electrons in Thin Films *Phys. Rev.* **106** 874-881

[51] Kamysbayev V, Filatov A S, Hu H, Rui X, Lagunas F, Wang D, Klie R F and Talapin D V 2020 Covalent surface modifications and superconductivity of two-dimensional metal carbide MXenes *Science* **369** 979-983

[52] Khazaei M, Arai M, Sasaki T, Chung C Y, Venkataramanan N S, Estili M, Sakka Y and Kawazoe Y 2013 Novel Electronic and Magnetic Properties of Two-Dimensional Transition Metal Carbides and Nitrides *Adv. Func. Mater.* **23** 2185-2192

[53] Bai Y, Zhou K, Srikanth N, Pang J H L, He X and Wang R 2016 Dependence of elastic and optical properties on surface terminated groups in two-dimensional MXene monolayers: a first-principles study *RSC Adv.* **6** 35731-35739

[54] Zha X H, Luo K, Li Q, Huang Q, He J, Wen X and Du S 2015 Role of the surface effect on the structural, electronic and mechanical properties of the carbide (MXenes) *EPL* **111** 26007

[55] Guo Z, Zhou J, Si C and Sun Z 2015 Flexible two-dimensional $Ti_{n+1}C_n$ (n = 1, 2 and 3) and their functionalized MXenes predicted by density functional theories *Phys. Chem. Chem. Phys.* **17** 15348-15354

[56] Fu Z H, Zhang Q F, Legut D, Si C, Germann T C, Lookman T, Du S Y, Francisco J S and Zhang R F 2016 Stabilization and strengthening effects of functional groups in two-dimensional titanium carbide *Phys. Rev. B* **94** 104103

[57] Tran M H, Schäfer T, Shahraei A, Dürrschnabel M, Molina-Luna L, Kramm U I and Birkel C S 2018 Adding a New Member to the MXene Family: Synthesis, Structure, and Electrocatalytic Activity for the Hydrogen Evolution Reaction of $V_4C_3T_x$ *ACS Appl. Energy Mater.* **1** 3908-3914

[58] Castro-Fernandez F R, Sellars C M and Whiteman J A 1985 Measurement of foil thickness and extinction distance by convergent beam transmission electron microscopy *Philosophical Magazine A* **52** 289-303

[59] Delille D, Pantel R and Van Cappellen E 2001 Crystal thickness and extinction distance determination using energy filtered CBED pattern intensity measurement and dynamical diffraction theory fitting *Ultramicroscopy* **87** 5-18

[60] Bergman D J 1978 The dielectric constant of a composite material-A problem in classical physics *Physics Reports* **43** 377-407